THE JOURNAL OF PHYSICAL CHEMISTRY B

pubs.acs.org/JPCB Article

Impact of Boundary Heat Losses on Frontal Polymerization

E. Goli, T. Gai, and P. H. Geubelle*

Cite This: https://dx.doi.org/10.1021/acs.jpcb.0c03107 Read Online

ACCESS | Metrics & More | Article Recommendations

ABSTRACT: Considered as a faster and energy-efficient alternative to conventional manufacturing techniques for thermosetting polymers and composites, frontal polymerization (FP) is built on a thermal equilibrium between the heat generated by the exothermic reaction of the resin system and the heat consumed by the advancing front. However, a heat loss to the surrounding may disrupt this thermal equilibrium and slow down and possibly quench the front. This paper investigates the impact of two types of heat loss to the surrounding on the key characteristics (propagation speed and maximum temperature) of the polymerization front: convective heat loss along of the boundary of the reaction channel and contact heat loss at channel-tool plate interfaces. The analysis is performed numerically using a nonlinear, adaptive fully coupled finite element solver.

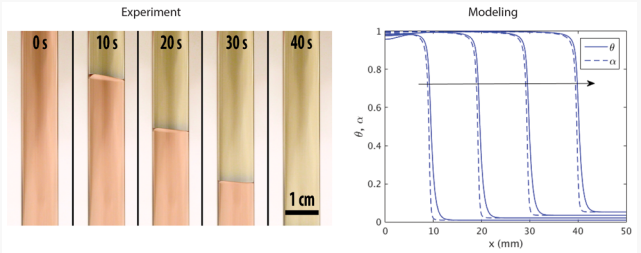

1. INTRODUCTION

Frontal polymerization (FP) is a self-sustained process wherein a localized polymerization front, fueled by the heat generated by the exothermic reaction of the monomer/catalyst solution, advances through the monomer by converting it into a polymer. While FP has been primarily applied to the manufacturing of thermosetting polymers,[1−7] more recent studies have focused on FP-based manufacturing of thermoset composites,[8−11] where it has been proposed as a faster, energy-efficient, and environmentally friendly alternative to current autoclave- and oven-based manufacturing techniques.

At the heart of the frontal polymerization process is the thermal equilibrium taking place between the heat generated by the exothermic reaction of the resin and the thermal diffusion occurring ahead of the propagating front. However, heat exchanges taking place between the reacting system and its surroundings may affect the thermal "reaction-diffusion equilibrium" and may have an impact on the key characteristics of the front, i.e., its propagation speed and maximum temperature.

Most analytical studies of FP available in the literature are performed in a 1-D setting[12−18] and do not involve the effects of heat losses along the boundary. Frulleni et al.[6] used the finite difference method to simulate FP in epoxy in a 2D channel with convective boundary conditions imposed along the edges of the channel. However, the convective heat transfer coefficient (sometimes referred to as "film coefficient") value adopted in that study was relatively small and the effect of heat loss on the system was minimal. Adopting a simplified first order kinetics model, Garbey and Tromeur-Dervout[19] proposed a specific use of domain decomposition to model quasi-planar unsteady fronts with applications in combustion and frontal polymerization. In a related study, Comissiong et al.[20] performed a 1-D semianalytical analysis and concluded that the presence of an inert layer can significantly affect propagation of the polymerization wave in a reactive layer due to the heat exchange between the two layers. More recently, Goli et al.[5] investigated the initiation and propagation of polymerization fronts in an acrylate-filled microchannel embedded in polydimethylsiloxane (PDMS). The results revealed a critical value of the channel radius below which the front cannot propagate due to the heat loss to the environment.

In this work, we perform a detailed parametric study of two heat loss mechanisms: (i) convective heat loss along the boundaries of a reacting channel, and (ii) contact heat loss via the channel/tool-plate interfaces. The analysis is performed in 2D by solving the coupled, transient thermo-chemical relations with the aid of an adaptive, nonlinear finite element solver. As illustrated hereafter, a substantial heat loss to the surroundings may greatly slow down and even quench the polymerization front. The parametric study is performed with a reacting channel filled with a dicyclopentadiene (DCPD) monomer with latent second-generation Grubbs catalyst, which serves as the reference material in previous studies.[8,4]

This manuscript is organized as follows: In section 2, we present a parametric study of the impact of heat convection

Received: April 7, 2020
Revised: June 17, 2020
Published: June 18, 2020

losses on the speed, temperature and shape of the front. We then carry out in section 3 a set of simulations to capture the effects of tool plates made of different materials covering a wide range of diffusivity and conductivity coefficients on the polymerization front. Section 3 also contained a study of the impact of a contact heat loss due to the contact between the reacting channel and a very large, perfectly conductive tool.

2. CONVECTIVE HEAT LOSS ALONG THE BOUNDARY

To analyze the effect of convective heat loss along the boundary, we solve the problem illustrated in Figure 1, which

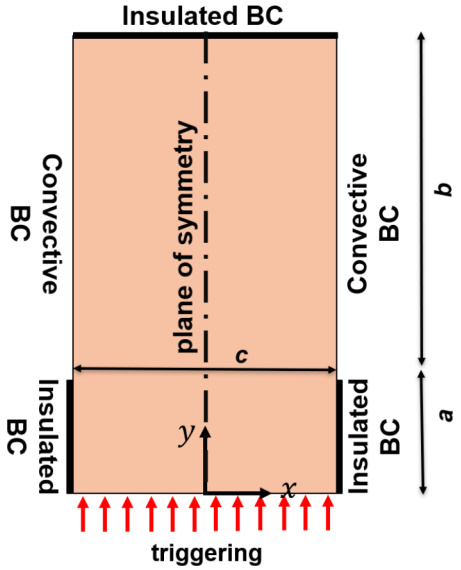

Figure 1. Problem configuration, dimensions, and boundary conditions for the study of the effect of convection boundary condition on the polymerization front.

involves a 2-D reaction channel of width c filled with a solution of dicyclopentadiene (DCPD) and 2nd-generation Grubbs catalyst. As indicated in ref 9, the initiation and propagation of the polymerization front can be described at the continuum level by the following system of partial differential equations (PDEs):where κ (in $\frac{W}{m\cdot K}$) denotes the thermal conductivity, C_p (in $\frac{J}{kg\cdot K}$) the specific heat, ρ (in $\frac{kg}{m^3}$) the density, and H_r (in $\frac{J}{kg}$) the total enthalpy of reaction. The second relation in (1) describes the cure kinetics associated with the exothermic reaction where A (in $\frac{1}{s}$) and E (in $\frac{J}{mol}$) are the pre-exponential factor and activation energy, respectively, while R (=8.314 $\frac{J}{mol\cdot K}$) is the universal gas constant. The classical Prout–Tompkins autocatalytic (PT) model, $(1-\alpha)^n\alpha^m$, with n and m denoting the orders of the reaction, is augmented by a diffusion factor, $(1+\exp[C(\alpha-\alpha_c)])^{-1}$, with the two constant parameters C and α_c introduced to capture the diffusion at higher temperatures.[21,9] The six cure kinetics parameters, A, E, n, m, C, and α_c, are obtained by nonlinear fitting of the evolution of the rate of cure obtained from differential scanning calorimetry (DSC) experiments.[9,8] The cure kinetics parameters and the physical/thermal properties entering (1) for the DCPD monomer studied in this work are presented in Table 1.

Table 1. Material and Cure Kinetics Properties of the DCPD Monomer

κ ($\frac{W}{m\cdot K}$)	ρ ($\frac{kg}{m^3}$)	C_p ($\frac{J}{kg\cdot K}$)	A ($\frac{1}{s}$)	E ($\frac{kJ}{mol}$)
0.15	980	1600	8.55e15	110.75
n	m	C	α_c	H_r ($\frac{J}{g}$)
1.72	0.77	14.48	0.41	350

$$\begin{cases} \kappa\left[\dfrac{\partial^2 T}{\partial x^2}+\dfrac{\partial^2 T}{\partial y^2}\right]+\rho H_r\dfrac{\partial \alpha}{\partial t}=\rho C_p\dfrac{\partial T}{\partial t}, \\ \dfrac{\partial \alpha}{\partial t}=A\exp\left(-\dfrac{E}{RT}\right)g(\alpha), \\ g(\alpha)=(1-\alpha)^n\alpha^m\dfrac{1}{1+\exp[C(\alpha-\alpha_c)]}, \end{cases} \quad (1)$$

The front is initiated from the bottom of the rectangular channel and propagates upward. A small (a = 2 mm) adiabatic region (i.e., with insulated lateral boundaries) is introduced to achieve a quasi-steady state of front propagation independent of the front initiation. Convective boundary conditions are applied along the remainder of the reaction channel (with b = 8 mm), while insulated conditions are applied along the top edge of the domain. The boundary and initial conditions complementing the PDEs (1) take the following form:

$$\begin{cases} T(x,y,0)=T_0, \text{ for } -\dfrac{c}{2}\le x\le\dfrac{c}{2}, 0\le y\le a+b, \\ \alpha(x,y,0)=\alpha_0, \text{ for } -\dfrac{c}{2}\le x\le\dfrac{c}{2}, 0\le y\le a+b, \\ T(x,0,t)=T_{trig}, \text{ for } -\dfrac{c}{2}\le x\le\dfrac{c}{2}, 0\le t\le t_{trig}, \\ \dfrac{\partial T}{\partial y}(x,0,t)=0, \text{ for } -\dfrac{c}{2}\le x\le\dfrac{c}{2}, t>t_{trig}, \\ \dfrac{\partial T}{\partial x}\left(\pm\dfrac{c}{2},y,t\right)=0, \text{ for } 0\le y\le a, t>0, \\ \dfrac{\partial T}{\partial y}(x,a+b,t)=0, \text{ for } -\dfrac{c}{2}\le x\le\dfrac{c}{2}, t>0, \\ \kappa\dfrac{\partial T}{\partial x}\left(\pm\dfrac{c}{2},y,t\right)=\mp h\left(T\left(\pm\dfrac{c}{2},y,t\right)-T_0\right), \text{ for } a<y\le a+b, t>0, \end{cases} \quad (2)$$

where T_{trig} refers to the triggering temperature that is applied to the bottom edge of the domain for a short period of time, t_{trig}, to initiate the front. T_0 and α_0 denote the initial temperature and the initial degree of cure, and they are set to 20 °C and 0.05, respectively, for all the simulations reported in this work. The convective heat transfer coefficient h (in $\frac{W}{m^2\cdot K}$) introduced to capture the heat convection loss typically takes values between between 10 to 100 $\frac{W}{m^2\cdot K}$ for systems exposed to low-velocity air flow.[22] For completeness, the parametric study presented hereafter considers values ranging from 0 to 200 $\frac{W}{m^2\cdot K}$.

The analysis of this problem starts by nondimensionalizing the time t, the spatial coordinate x, and the temperature T by

https://dx.doi.org/10.1021/acs.jpcb.0c03107
J. Phys. Chem. B XXXX, XXX, XXX−XXX

$$\tau = At, \quad \tilde{x} = \frac{x}{L}, \quad \tilde{y} = \frac{y}{L}, \quad \theta = \frac{T - T_0}{T_{max} - T_0} \tag{3}$$

where $L = \sqrt{\frac{\kappa}{\rho A C_p}}$ is the intrinsic length scale for this problem, and $T_{max} = T_0 + \frac{H_r(1-\alpha_0)}{C_p}$ denotes the adiabatic temperature associated with the front. Substituting (3) into (1) yields

$$\begin{cases} \left[\frac{\partial^2\theta}{\partial\tilde{x}^2} + \frac{\partial^2\theta}{\partial\tilde{y}^2}\right] + \frac{\partial\alpha}{\partial\tau} = \frac{\partial\theta}{\partial\tau}, \\ \frac{\partial\alpha}{\partial\tau} = \exp\left(-\frac{\beta}{\theta+\gamma}\right) g(\alpha), \end{cases} \tag{4}$$

where

$$\begin{cases} \beta = -\frac{EC_p}{RH_r}, \\ \gamma = \frac{T_0 C_p}{H_r}, \end{cases} \tag{5}$$

are dimensionless parameters that capture the effect of the activation energy E and initial temperature T_0, respectively. The BCs in (2) can be rewritten as

$$\begin{cases} \theta(\tilde{x}, \tilde{y}, 0) = 0, \text{ for } -\frac{c}{2L} \le \tilde{x} \le \frac{c}{2L}, 0 \le \tilde{y} \le \frac{a+b}{L}, \\ \alpha(\tilde{x}, \tilde{y}, 0) = \alpha_0, \text{ for } -\frac{c}{2L} \le \tilde{x} \le \frac{c}{2L}, 0 \le \tilde{y} \le \frac{a+b}{L}, \\ \theta(\tilde{x}, 0, \tau) = \theta_{trig}, \text{ for } -\frac{c}{2L} \le \tilde{x} \le \frac{c}{2L}, 0 \le \tau \le \tau_{trig}, \\ \frac{\partial\theta}{\partial\tilde{y}}(\tilde{x}, 0, \tau) = 0, \text{ for } -\frac{c}{2L} \le \tilde{x} \le \frac{c}{2L}, \tau > \tau_{trig}, \\ \frac{\partial\theta}{\partial\tilde{x}}\left(\pm\frac{c}{2L}, \tilde{y}, \tau\right) = 0, \text{ for } 0 \le \tilde{y} \le \frac{a}{L}, \tau > 0, \\ \frac{\partial\theta}{\partial\tilde{y}}\left(\tilde{x}, \frac{a+b}{L}, \tau\right) = 0, \text{ for } -\frac{c}{2L} \le \tilde{x} \le \frac{c}{2L}, \tau > 0, \\ \frac{\partial\theta}{\partial\tilde{x}}\left(\pm\frac{c}{2L}, \tilde{y}, \tau\right) = \mp\delta\theta\left(\pm\frac{c}{2L}, \tilde{y}, \tau\right), \text{ for } \frac{a}{L} \le \tilde{y} \le \frac{a+b}{L}, \tau > 0, \end{cases} \tag{6}$$

where δ is the nondimensional convection parameter defined as

$$\delta = \frac{hL}{\kappa} \tag{7}$$

Numerical modeling of the advancing polymerization front is challenging as an h-adaptivity module is needed to capture the sharp gradients in temperature and degree of cure in the vicinity of the advancing front. Here, we adopt the Multi-physics Object-Oriented Simulation Environment,[23] an open source C++ math library that provides mesh adaptivity. The solver involves an adaptive implicit Euler time integration scheme and a Jacobian-free Newton–Krylov[24−26] preconditioner to solve the linearized system of equations at each iteration. The simulations presented hereafter are performed in 2-D. The formulation and finite element framework are readily extended to 3-D problems, the increased computational cost of which is mitigated by the robust mesh adaptivity module and adopted preconditioned Jacobean-free scheme.

Here we carry out a parametric study consisting of 121 2-D simulations with different values for the channel width (c = 1, 1.5, 2, 3, 4, 5, 6, 7, 8, 9, and 10 mm) and the convective heat transfer coefficient (h = 0, 20, 40, 60, ..., 200 $\frac{W}{m^2 \cdot K}$). For all the simulations reported in this work, t_{trig}, T_{trig}, and Δt are set to 1 s, 190 °C, and 0.01 s, respectively. The element size for the initially uniform mesh of quadrilateral elements, before the mesh adaptivity module is activated, and the maximum level of mesh adaptivity are $1e-5$ m and 3, respectively. Taking advantage of symmetry, we solve the problem on half of the domain ($0 \le x \le c/2$). Typical simulations presented hereafter take approximately 8 h to run in parallel on a 56-core Dell mini-server with CentOS 7.7 distribution of Linux OS.

Figure 3 complements Figure 2 by providing more details for the cases with h = 0, 60, and 160 $\left(\frac{W}{m^2 \cdot K}\right)$. Figure 3a shows the temperature profiles along the line of symmetry at t = 4 and 8 s and illustrates how the heat loss behind the front lowers the temperature gradient and hinders the polymerization. The evolution of the front location is presented in Figure 3b, with the slope of the lines denoting the front velocity. The location of the front at each time step is extracted as the y-coordinate of the node with α = 0.5 along the symmetry line (x = 0). The straight trajectory curves indicate a steady-state regime for the front. In the remainder of this section, the front speed will be computed over the spatial window 5 mm $\le y \le$ 7 mm.

The convection heat loss to the surrounding also affects the maximum degree of cure in the channel, especially in the vicinity of the channel boundary. This fact is illustrated in Figure 4, which presents snapshots of the spatial variation of the degree of cure computed along the center line and edge of the channels at times t = 4 s and t = 8 s for the case c = 1 mm and h = 160 $\frac{W}{m^2 \cdot K}$.

The front velocity and maximum temperature values obtained from this parametric study are presented in Figure 5. As apparent there, lowering the resin volume and increasing the convection coefficient reinforce the diffusion component of the reaction-diffusion system, thereby decreasing the maximum temperature gradient, front velocity, and ultimately quenching the front as observed in the cases with c = 1 mm and h = 180 and 200 $\frac{W}{m^2 \cdot K}$. As expected, the effects are more intense for the narrower channels.

For a given solution of monomer and catalyst, the problem can be described by two key nondimensional parameters: the nondimensional channel width $\frac{c}{L}$ and nondimensional convection parameter δ. To summarize the results of the parametric study, we present in Figure 6 a "master curve" that captures the effects of the two parameters combined in the form of a power law.

3. CONTACT HEAT LOSS ALONG THE INTERFACE

We now turn our attention to the impact on the front characteristics of the heat loss taking place along the contact interface between the resin channel and a tool plate (Figure 7). As previously, a small insulated region (a = 2 mm and

https://dx.doi.org/10.1021/acs.jpcb.0c03107
J. Phys. Chem. B XXXX, XXX, XXX−XXX

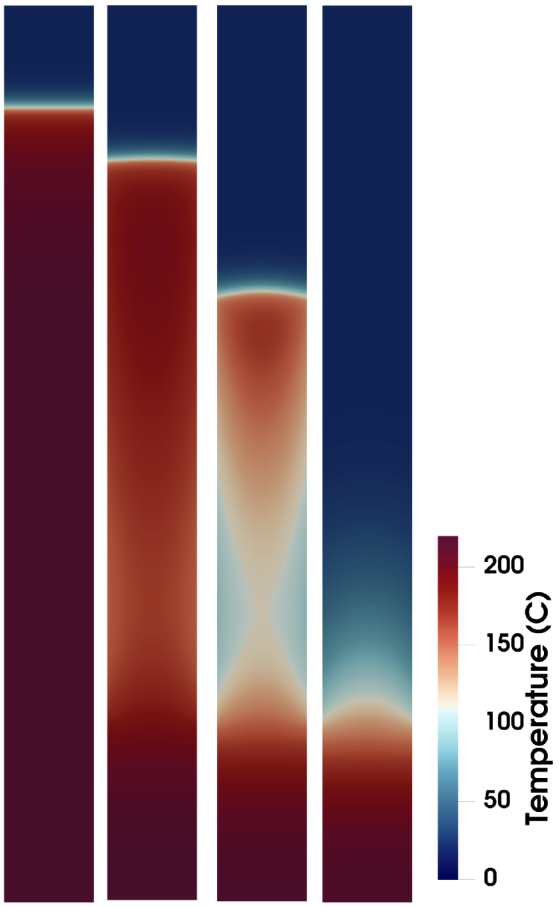

Figure 2. Temperature contours computed at t = 8 s for the case of a narrow DCPD channel with c = 1 mm, showing from left to right a stable and flat-shape front $\left(h = 0\ \frac{\mathrm{W}}{\mathrm{m}^2\cdot\mathrm{K}}\right)$, a curved-shape front $\left(h = 60\ \frac{\mathrm{W}}{\mathrm{m}^2\cdot\mathrm{K}}\right)$, a "detached" front $\left(h = 160\ \frac{\mathrm{W}}{\mathrm{m}^2\cdot\mathrm{K}}\right)$, and a quenched front $\left(h = 200\ \frac{\mathrm{W}}{\mathrm{m}^2\cdot\mathrm{K}}\right)$.

$\kappa = 0\ \frac{\mathrm{W}}{\mathrm{m}\cdot\mathrm{K}}$) is introduced to ensure that the simulated front has reached a steady-state regime before entering the contact interface with the plate. The plate length is set long enough (b = 18 mm) to achieve steady-state propagation of the front in the region in contact with the tool plate. All exterior boundaries are assumed to be insulated. Rewriting (4) for the tool plate yields

$$\frac{\partial^2\theta}{\partial\tilde{x}^2} + \frac{\partial^2\theta}{\partial\tilde{y}^2} = \frac{\lambda_m}{\lambda_p}\frac{\partial\theta}{\partial\tau} \tag{8}$$

where $\lambda = \frac{\kappa}{\rho C_p}$ denotes the thermal diffusivity, and subscripts m and p refer to the monomer and the tool plate, respectively. As previously, taking advantage of symmetry, we solve the problem on half of the domain ($0 \le x \le c/2$). The continuity of heat flux along the monomer-plate interface is described by

$$\frac{\partial\theta}{\partial\tilde{x}}\left(\frac{c^-}{2L}, \tilde{y}, \tau\right) = \frac{\kappa_p}{\kappa_m}\frac{\partial\theta}{\partial\tilde{x}}\left(\frac{c^+}{2L}, \tilde{y}, \tau\right), \tag{9}$$

where superscripts $^-$ and $^+$ denote the left and right sides of the interface, respectively. Therefore, given a fixed chemical composition for the monomer solution and a fixed plate width, the contact heat loss during polymerization is a function of three nondimensional parameters: $\tilde{\lambda} = \frac{\lambda_p}{\lambda_m}$, $\tilde{\kappa} = \frac{\kappa_p}{\kappa_m}$, and $\frac{c}{L}$, which are the focus of the parametric study presented hereafter.

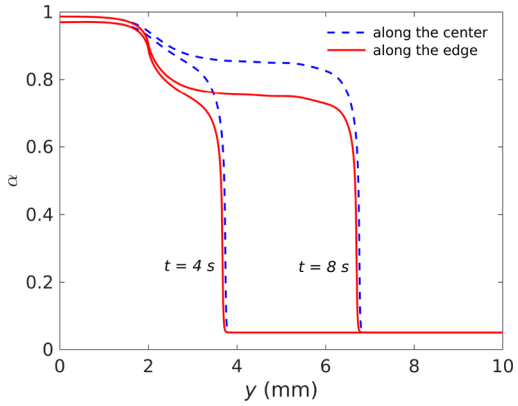

Figure 4. Degree of cure profiles at t = 4 s and t = 8 s along the center and edge of the channel for the case c = 1 mm and $h = 160\ \frac{\mathrm{W}}{\mathrm{m}^2\cdot\mathrm{K}}$.

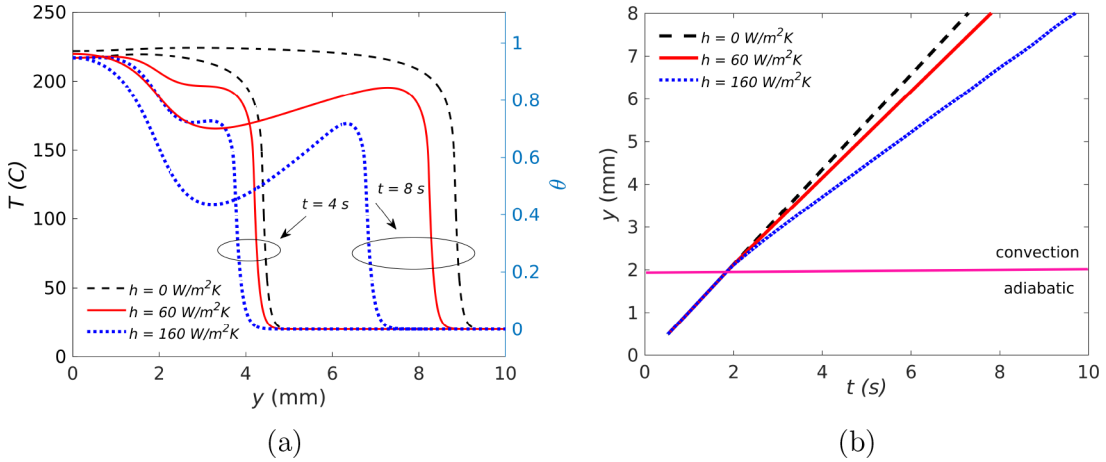

Figure 3. For the cases with c = 1 mm and h = 0, 60, and 160 $\frac{\mathrm{W}}{\mathrm{m}^2\cdot\mathrm{K}}$: (a) Temperature curves extracted along the line of symmetry (x = 0, 0 ≤ y ≤ 0.01 m) at t = 4 and 8 s. (b) Front trajectories, showing the slowdown of the front after it enters the convection BC zone.

https://dx.doi.org/10.1021/acs.jpcb.0c03107
J. Phys. Chem. B XXXX, XXX, XXX−XXX

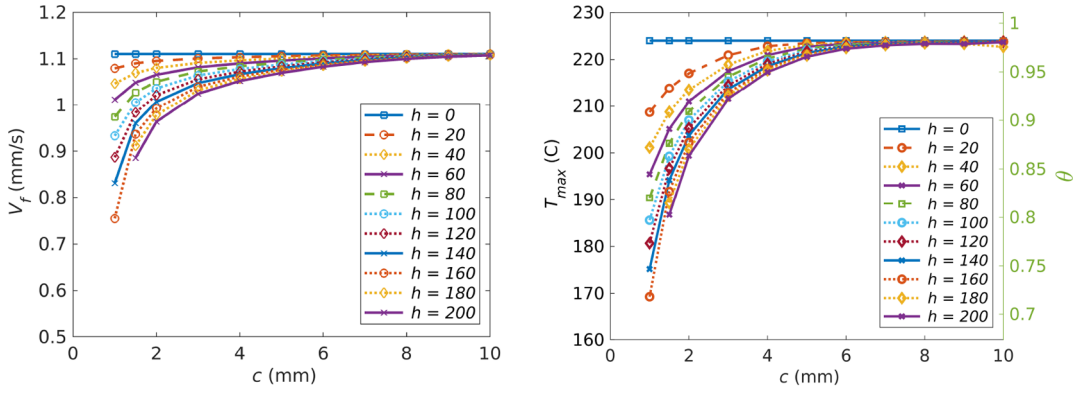

Figure 5. Effect of the convection coefficient, h, and the channel width, c, on (a) the front velocity, V_f, and (b) the maximum temperature, T_{max}. Reducing the convective heat transfer coefficient value and/or adopting a wider channel yields a faster polymerization front. The h values are given in $\frac{W}{m^2 \cdot K}$.

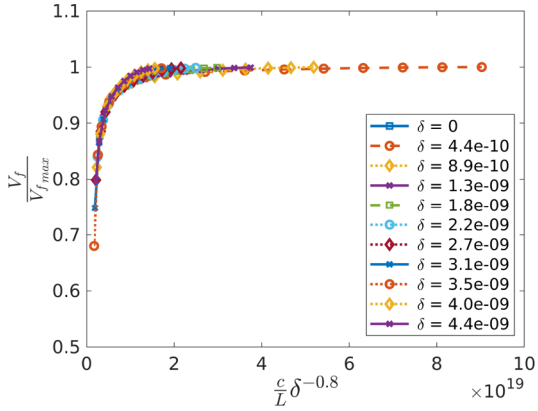

Figure 6. "Master front velocity curve" expressed in terms of the nondimensional channel width $\frac{c}{L}$ and the nondimensional convection parameter δ defined in (7).

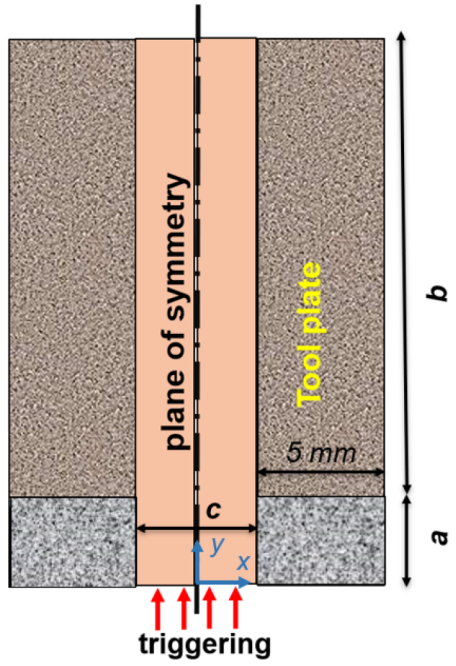

Figure 7. Problem configuration, dimensions, and boundary conditions for the study of the effect of contact boundary condition on the polymerization front.

In this study, we adopt the following ranges for the diffusivity and conductivity ratios:

$$\begin{cases} 0.1 \le \widetilde{\lambda} \le 10, \\ 0.01 \le \widetilde{\kappa} \le 10. \end{cases} \tag{10}$$

Recalling that the thermal properties of DCPD are λ_m = 9.69e−8 $\frac{m^2}{s}$ and κ_m = 0.152 $\frac{W}{m \cdot K}$, these ranges include tool plates made of polydimethylsiloxane (PDMS) ($\widetilde{\lambda}$ = 1.45, $\widetilde{\kappa}$ = 1.38), pDCPD ($\widetilde{\lambda}$ = 1, $\widetilde{\kappa}$ = 1), and silica aerogel ($\widetilde{\lambda}$ = 1.23, $\widetilde{\kappa}$ = 0.02).

The contour plots shown in Figure 8a−c present the values of front velocity extracted from this parametric study for the cases with $\widetilde{\lambda}$ = 0.1, 1, and 10. Each plot demonstrates how different combinations of resin volume and conductivity ratio, $\widetilde{\kappa}$, affect the velocity of the front. The dark blue area on the upper-left of the figures denotes the combinations of channel width and conductivity ratio that result in a quenching front, for which the combination of heat diffusion inside the channel and heat loss to the plate surpasses the heat generated by the exothermic reaction of resin solution. The highest values of front velocity are associated with the cases corresponding with wide channels and thermally insulating plates (i.e., low $\widetilde{\kappa}$).

As shown in Figure 8d, the impact of the diffusivity and conductivity of the plate relative to those of the channel is somewhat complex. For the cases corresponding to lower relative diffusivity ($\widetilde{\lambda}$ = 0.1 and 1) an increase in relative conductivity $\widetilde{\kappa}$ leads to a monotonic decrease in the front velocity. For the case $\widetilde{\lambda}$ = 10 (blue curve in Figure 8d), however, increasing $\widetilde{\kappa}$ first leads to an increase in front velocity, until $\widetilde{\kappa}$ > 1 at which point the increased conductivity of the plate makes it a heat sink, thereby slowing down the front.

For a fixed channel width (c = 4 mm), Figure 9 presents snapshots of the thermal profile of the polymerization front at t = 12 s for four extreme cases, demonstrating how the diffusivity and conductivity ratios affect the front shape and speed. As is apparent in parts c and d of Figure 9, higher values of λ_p leads to heat losses to the plate as soon as the front leaves

https://dx.doi.org/10.1021/acs.jpcb.0c03107
J. Phys. Chem. B XXXX, XXX, XXX−XXX

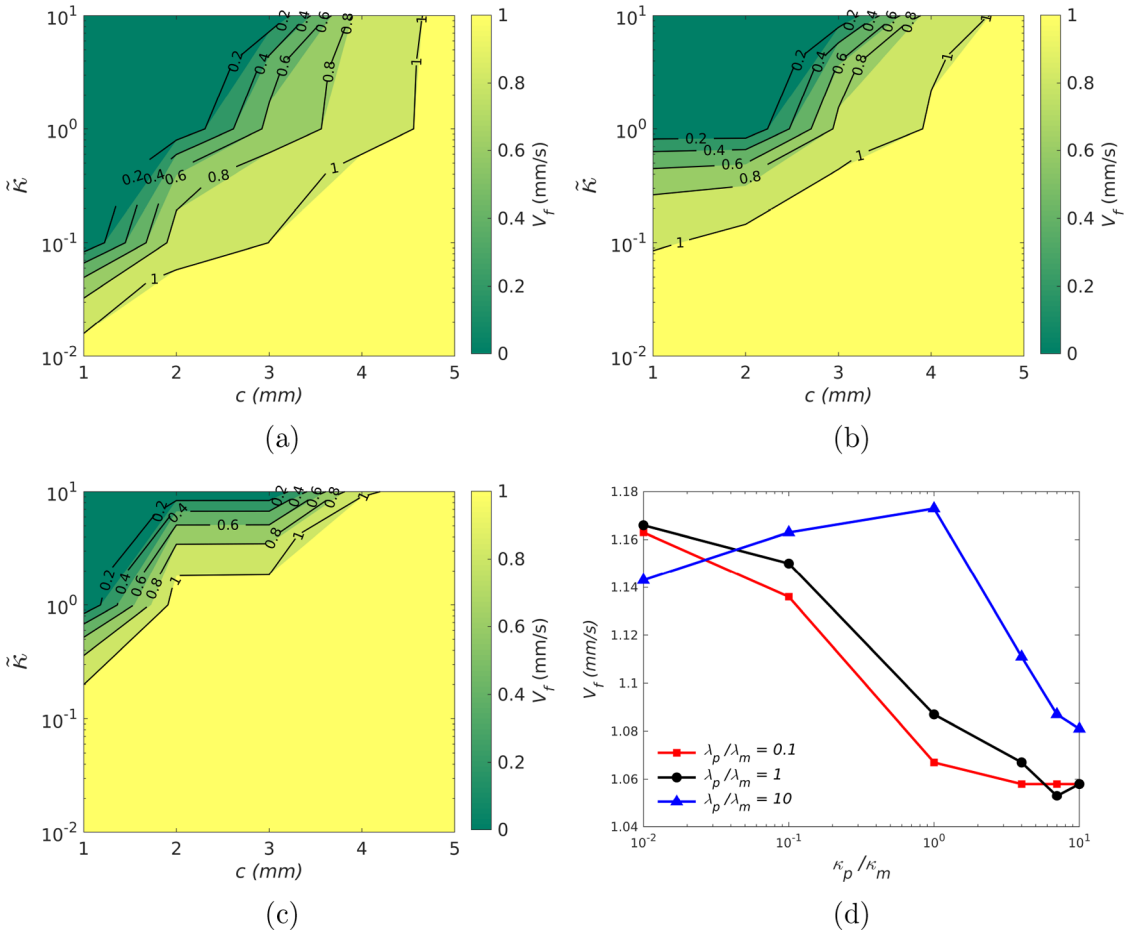

Figure 8. Front velocity in $(c, \tilde{\kappa})$ space corresponding to (a) $\tilde{\lambda}$ = 0.1, (b) $\tilde{\lambda}$ = 1, and (c) $\tilde{\lambda}$ = 10. (d) Dependence of the front velocity on the conductivity ratios for three values of the diffusivity ratios.

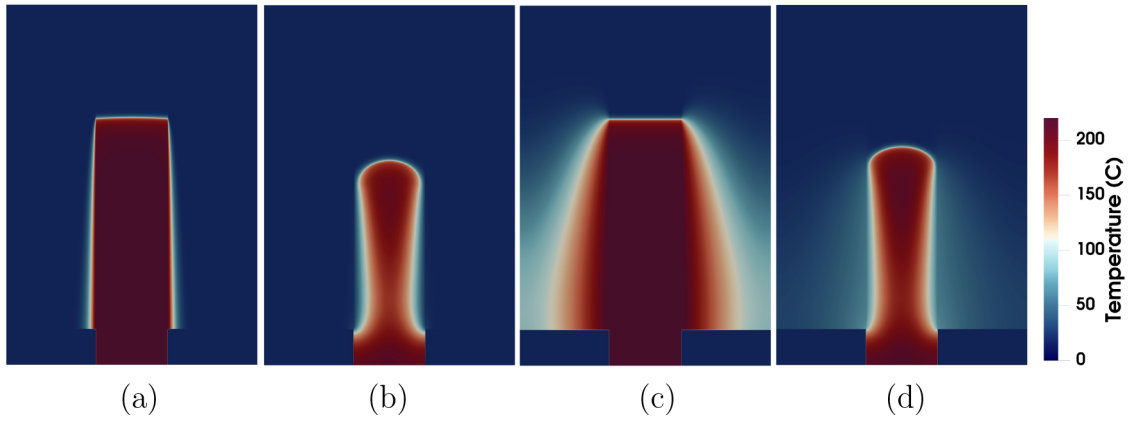

Figure 9. Temperature field computed at t = 12 s for a polymerization front in a 4 mm-wide-channel of DCPD for $(\tilde{\lambda}, \tilde{\kappa})$ equal to (a) (0.1, 0.01), (b) (0.1, 10), (c) (10, 0.01), and (d) (10, 10).

the adiabatic region. Conversely, systems with lower plate diffusivity values (parts a and b of Figure 9) are characterized by very small losses to the surrounding medium and thereby yield sharper polymerization fronts.

In addition to the plate material, the volume of available resin in the channel plays a crucial role in preserving the heat balance involved in the reaction-diffusion process. Figure 10 shows the temperature profiles and trajectories of the front along the line of symmetry for the cases with c = 5 mm (dashed curves) and 3 mm (solid curves). For both values of the channel width, the relative conductivity and diffusivity are chosen to be $\tilde{\kappa}$ = 1 and $\tilde{\lambda}$ = 0.1. As the channel width decreases, the heat loss in the surroundings plays an increasing role in reducing the energy available for the propagation of the front, thereby substantially reducing the front speed, as is apparent in Figure 10b.

To conclude this study, we investigate the limiting case of a very large plate of initial temperature T_0 with infinite

https://dx.doi.org/10.1021/acs.jpcb.0c03107
J. Phys. Chem. B XXXX, XXX, XXX−XXX

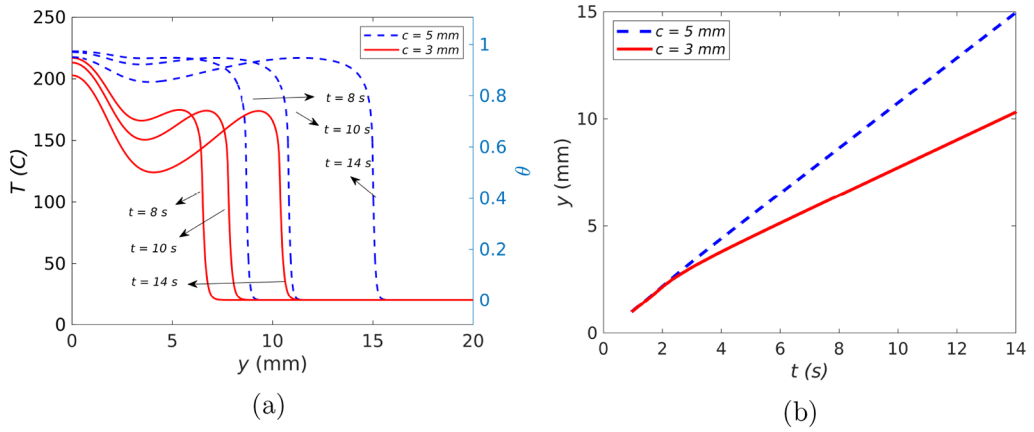

Figure 10. (a) Temperature profiles at t = 8, 10, and 14 s and (b) front trajectories along the line of symmetry for the cases with c = 5 (dashed curves) and 3 mm (solid curves), with $\tilde{\kappa}$= 1 and $\tilde{\kappa}$= 0.1.

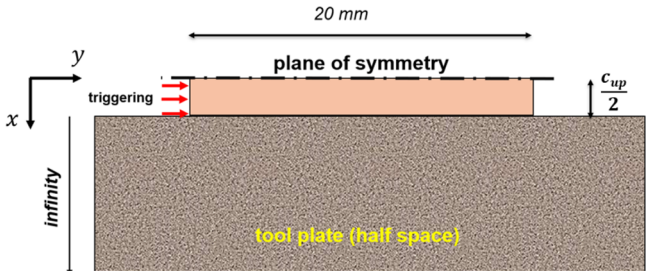

Figure 11. Limiting case: Channel of DCPD monomer placed on top of a half space with infinite diffusivity, reducing the channel/plate interface condition to the Dirichlet condition $T(c_{up}/2, y, t) = T_0$.

diffusivity, for which the thermal boundary condition can be reduced to the Dirichlet (fixed temperature) condition $T(c_{up}/2, y, t) = T_0$ along the plate/channel interface, as illustrated in Figure 11. Of particular interest in this final study is the existence of a critical value of the channel width c_{up} above which a polymerization front is able to propagate in the channel although the edges of the channel are fixed at T_0.

A parametric study of the channel width yields the critical value c_{up} = 3.1 mm for the same chemistry and initial conditions as in section 2. Figure 12 shows snapshots of the temperature and degree-of-cure fields associated with the polymerization front at t = 25 s. Note that the channel is chosen long enough to make the results independent of the transient phase associated with the triggering of the polymerization process. As is apparent in Figure 12(top), the temperature rise generated by the propagating front is rapidly absorbed by the contacting plate. However, as illustrated in Figure 12(bottom), a layer of uncured resin serves as an insulating "boundary layer", thereby allowing most of the channel to be cured. As expected, the critical value of the channel width varies with T_0 with c_{up} = 2.6 and 3.8 mm for T_0 = 25 and 15 °C, respectively.

4. CONCLUSIONS

We have performed a finite element analysis of the impact of boundary heat losses on the speed and shape of a polymerization front propagating in a channel of DCPD. Two types of boundary conditions have been analyzed. The first analysis pertained to convective heat losses along the channel boundary, with emphasis on capturing the effect of the convective heat transfer coefficient and channel thickness on the speed and maximum temperature of the front. A sharp transition was obtained between the adiabatic/large-channel solution and the high-convective-loss/narrow-channel cases for which the front is quenched. The second analysis involved the heat losses associated with a contacting plate, for which the solution was expressed in terms of the diffusivity and thermal conductivity ratios between the resin and the plate, and the channel width. The parametric study showed a sharp transition between the quenched and adiabatic states. In the limiting case

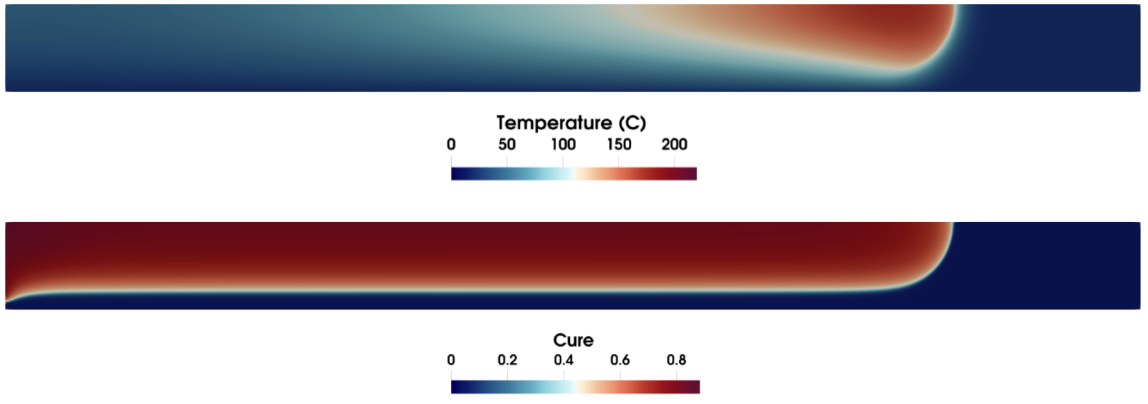

Figure 12. Temperature (top) and degree of cure (bottom) contours at t = 25 s, showing the insulating effect of the uncured monomer layer in the vicinity of the plate (c_{up} = 3.1 mm and T_0= 20 °C).

https://dx.doi.org/10.1021/acs.jpcb.0c03107
J. Phys. Chem. B XXXX, XXX, XXX−XXX

of a very large plate of infinite diffusivity, frontal polymerization is achievable in spite of the large heat losses to the plate due to the insulation associated with a boundary layer of uncured resin created along the plate boundary.

AUTHOR INFORMATION

Corresponding Author

P. H. Geubelle − *Department of Aerospace Engineering and United States Beckman Institute for Advanced Science and Technology, University of Illinois, Urbana, Illinois 61801, United States;* orcid.org/0000-0002-4670-5474; Phone: +1(217)244-7648; Email: geubelle@illinois.edu

Authors

E. Goli − *Department of Civil and Environmental Engineering and United States Beckman Institute for Advanced Science and Technology, University of Illinois, Urbana, Illinois 61801, United States;* orcid.org/0000-0002-9782-7789

T. Gai − *Department of Aerospace Engineering, University of Illinois, Urbana, Illinois 61801, United States*

Complete contact information is available at: https://pubs.acs.org/10.1021/acs.jpcb.0c03107

Notes

The authors declare no competing financial interest.

ACKNOWLEDGMENTS

This work was supported by the Air Force Office of Scientific Research through Award FA9550-16-1-0017 (Dr. B. "Les" Lee, Program Manager) as part of the Center for Excellence in Self-Healing, Regeneration, and Structural Remodeling. The authors also acknowledge the support of the National Science Foundation, Grant No. 1830635, through the LEAP HI: Manufacturing USA Program.

REFERENCES

(1) Pojman, J. A.; Curtis, G.; Ilyashenko, V. M. Ilyashenko, Frontal polymerization in solution. *J. Am. Chem. Soc.* **1996**, *118* (15), 3783−3784.

(2) Pojman, J. A.; Ilyashenko, V. M.; Khan, A. M. Free-radical frontal polymerization: self-propagating thermal reaction waves. *J. Chem. Soc., Faraday Trans.* **1996**, *92* (16), 2825−2837.

(3) Khan, A. M.; Pojman, J. A. The use of frontal polymerization in polymer synthesis. *Trends Polym. Sci.* **1996**, *8* (4), 253−257.

(4) Goli, E.; Robertson, I.; Geubelle, P.; Moore, J. Frontal polymerization of dicyclopentadiene: A numerical study. *J. Phys. Chem. B* **2018**, *122* (16), 4583.

(5) Goli, E.; Robertson, I. D.; Agarwal, H.; Pruitt, E. L.; Grolman, J. M.; Geubelle, P. H.; Moore, J. S. Frontal polymerization accelerated by continuous conductive elements. *J. Appl. Polym. Sci.* **2019**, *136* (17), 47418.

(6) Frulloni, E.; Salinas, M. M.; Torre, L.; Mariani, A.; Kenny, J. M. Numerical modeling and experimental study of the frontal polymerization of the diglycidyl ether of bisphenol a/diethylenetriamine epoxy system. *J. Appl. Polym. Sci.* **2005**, *96*, 1756−1766.

(7) Ivanov, V.; Mel'nikov, V.; Stegno, E. On two modes of the frontal polymerization of methyl methacrylate. *Russ. J. Phys. Chem. B* **2009**, *3* (4), 672−673.

(8) Robertson, I. D.; Yourdkhani, M.; Centellas, P. J.; Aw, J. E.; Ivanoff, D. G.; Goli, E.; Lloyd, E. M.; Dean, L. M.; Sottos, N. R.; Geubelle, P. H.; et al. Rapid energy-efficient manufacturing of polymers and composites via frontal polymerization. *Nature* **2018**, *557* (7704), 223.

(9) Goli, E.; Parikh, N. A.; Yourdkhani, M.; Hibbard, N. G.; Moore, J. S.; Sottos, N. R.; Geubelle, P. H. Frontal polymerization of unidirectional carbon-fiber-reinforced composites. *Composites, Part A* **2020**, *130*, 105689.

(10) Vyas, S.; Goli, E.; Zhang, X.; Geubelle, P. Manufacturing of unidirectional glass-fiber-reinforced composites via frontal polymerization: A numerical study. *Compos. Sci. Technol.* **2019**, *184*, 107832.

(11) Goli, E.; Parikh, N. A.; Vyas, S. K.; Zhang, X.; Sottos, N. R.; Moore, J. S.; Geubelle, P. H., Manufacturing of carbon- and glass-fiber composites using frontal polymerization. In: *ICCM22 2019*. Engineers Australia, Melbourne, Australia, 2019; pp 1509−1517.

(12) Goldfeder, P.; Volpert, V. A.; Ilyashenko, V.; Khan, A.; Pojman, J.; Solovyov, S. Mathematical modeling of free-radical polymerization fronts. *J. Phys. Chem. B* **1997**, *101* (18), 3474−3482.

(13) Goldfeder, P. M.; Volpert, V. A. Nonadiabatic frontal polymerization. *J. Eng. Math.* **1998**, *34* (3), 301−318.

(14) Viner, V. G.; Pojman, J. A.; Golovaty, D. The effect of phase change materials on the frontal polymerization of a triacrylate. *Phys. D* **2010**, *239* (11), 838−847.

(15) Cardarelli, S. A.; Golovaty, D.; Gross, L.; Gyrya, V. T.; Zhu, J. A numerical study of one-step models of polymerization: Frontal versus bulk mode. *Phys. D* **2005**, *206* (3−4), 145−165.

(16) Comissiong, D. M.; Gross, L. K.; Volpert, V. A. Nonlinear dynamics of frontal polymerization with autoacceleration. *J. Eng. Math.* **2005**, *53*, 59−78.

(17) Devadoss, D. E.; Pojman, J. A.; Volpert, V. A. Mathematical modeling of thiol-ene frontal polymerization. *Chem. Eng. Sci.* **2006**, *61*, 1261−1275.

(18) Golovaty, D. On step-function reaction kinetics model in the absence of material diffusion. *SIAM J. Appl. Math.* **2007**, *67*, 792−809.

(19) Garbey, M.; Tromeur-Dervout, D. A new parallel solver for the nonperiodic incompressible navier−stokes equations with a fourier method: Application to frontal polymerization. *J. Comput. Phys.* **1998**, *145* (1), 316−331.

(20) Comissiong, D.; Gross, L.; Volpert, V. Frontal polymerization in the presence of an inert material. *J. Eng. Math.* **2006**, *54* (4), 389−402.

(21) Yang, G.; Lee, J. K. Curing kinetics and mechanical properties of endo-dicyclopentadiene synthesized using different Grubbs' catalysts. *Ind. Eng. Chem. Res.* **2014**, *53* (8), 3001−3011.

(22) Rohsenow, W. M.; Hartnett, J. P.; Cho, Y. I., et al., *Handbook of heat transfer*, McGraw-Hill: New York, 1998; Vol. *3*.

(23) Gaston, D.; Newman, C.; Hansen, G.; Lebrun-Grandié, D. Moose: A parallel computational framework for coupled systems of nonlinear equations. *Nucl. Eng. Des.* **2009**, *239*, 1768−1778.

(24) Knoll, D. A.; Keyes, D. E. Jacobian-free Newton Krylov methods: A survey of approaches and applications. *J. Comput. Phys.* **2004**, *193*, 357−397.

(25) Pernice, M.; Walker, H. Nitsol: A Newton iterative solver for nonlinear systems. *SIAM Journal on Scientific Computing* **1998**, *19*, 302−318.

(26) May, D. A.; Brown, J.; Le Pourhiet, L. A scalable, matrix-free multigrid preconditioner for finite element discretizations of heterogeneous stokes flow. *Computer Methods in Applied Mechanics and Engineering* **2015**, *290*, 496−523.